Title

Tracking ultrafast non-adiabatic dissociation dynamics of the deuterated water dication molecule.

Journal

The Journal of chemical physics, 161(4)

ISSN

0021-9606

Authors

Iskandar, W

Rescigno, TN

Orel, AE

et al.

Publication Date

2024-07-01

DOI

10.1063/5.0219029

Peer reviewed

Tracking ultrafast non-adiabatic dissociation dynamics of the deuterated water dication molecule

W. Iskandar,[1] T. N. Rescigno,[1] A. E. Orel,[2] K. A. Larsen,[1,3] T. Severt,[4] Z. L. Streeter,[1,5] B. Jochim,[4] B. Griffin,[1,6] D. Call,[6] V. Davis,[6] C. W. McCurdy,[1,5] R. R. Lucchese,[1] J. B. Williams,[6] I. Ben-Itzhak,[4] D. S. Slaughter,[1] and Th. Weber[1,*]

[1] *Chemical Sciences Division, Lawrence Berkeley National Laboratory, Berkeley, CA-94720, USA*
[2] *Chemical Engineering, University of California, Davis, CA-95616, USA*
[3] *Graduate Group in Applied Science and Technology, University of California, Berkeley, USA*
[4] *J. R. Macdonald Laboratory, Department of Physics, Kansas State University, Manhattan, KS-66506, USA*
[5] *Department of Chemistry, University of California, Davis, CA-95616, USA*
[6] *Department of Physics, University of Nevada, Reno, NV-89557, USA*

(Dated: July 1, 2024)

We applied reaction microscopy to elucidate fast non-adiabatic dissociation dynamics of deuterated water molecules after direct photo-double ionization at 61 eV with synchrotron radiation. For the very rare $D^+ + O^+ + D$ breakup channel, the particle momenta, angular, and energy distributions of electrons and ions, measured in coincidence, reveal distinct electronic dication states and their dissociation pathways via spin-orbit coupling and charge transfer at crossings and seams on the potential energy surfaces. Notably, we could distinguish between direct and fast sequential dissociation scenarios. For the latter case, our measurements reveal the geometry and orientation of the deuterated water molecule with respect to the polarization vector that lead to this rare 3-body molecular breakup channel. Aided by multi-reference configuration-interaction calculations, the dissociation dynamics could be traced on the relevant potential energy surfaces and in particular their crossings and seams. This approach also unraveled the ultrafast time scales governing these processes.

PACS numbers: 32.80.-t,33.60.+q, 33.80.-b,36.40.-c,82.50.Hp

I. INTRODUCTION

Non-adiabatic dissociation processes in molecules initiated by excitation or ionization involve excited-state dynamics beyond the Born-Oppenheimer approximation as, in the presence of the electrons, nuclear motion takes place on more than one potential energy surface (PES) [1–4]. Non-radiative transitions between the surfaces are mainly facilitated via Internal Conversion (IC) or Inter System Crossing (ISC). ISC is a process of interest in photochemistry and photobiology [5–9], but it is much less understood in polyatomic molecules than IC. In contrast to IC, which is spin-conserving, ISC is a non-adiabatic transition of the molecule from one electronic state to another that requires Spin-Orbit Coupling (SOC) and, as such, is spin-nonconserving. SOC is a relativistic effect and is at the heart of non-adiabatic molecular transitions because it enables electron transfer at favorable geometries. In turn, the electron transfer changes the dissociation process, exemplifying the coupling between the electronic and nuclear part of the dynamics. The spin-orbit interaction in non-adiabatic transitions can, therefore, open new reaction pathways that may compete with IC.

SOC in molecules comprised of first-row atoms is generally weak, and therefore favorable conditions are required to yield effective transition rates. That means ISC requires adequate time for the coupling to take place; time which is provided for in potential wells of metastable electronic states [10] or between states that run flat and in parallel asymptotically. For faster dynamical processes, which (for example) take place after doubly ionizing molecules, adequate wells, seams, or parallel states, along which the PESs are coupled, have to be present at intermediate molecular geometries and persist for enough time until SOC is outpaced by competing dissociation scenarios. Observing and quantifying these rare ultrafast transitions is very challenging, as various reaction pathways have to be traced and transient states have to be identified.

Following the fragmentation processes in adequate detail requires highly differential investigations that are able to unravel the evolution of molecular degrees of freedom such as bending and stretching modes for specific electronic states during the dissociation. In order to successfully address these challenges, it is important to choose a fundamental molecule that is within reach of both complete experimental characterization and accurate theoretical treatment and interpretation. The double ionization of water, followed by the breakup of the dication, is an ideal system in which to study such ultrafast fundamental dynamics that depends on SOC in great detail. While SOC in a single molecule often contributes only on the few- or sub-percent level, such scarce outcomes can aggregate in dense matter, which for in-

* TWeber@lbl.gov

stance contains a lot of water molecules, and result in spin-forbidden relaxation pathways and (i.a., harmful) products in chemical reactions that, e.g., cause unwanted defects or cell damages, and as such have notable affects.

State-selective investigations of the nuclear dynamics of water molecules upon photoionization are still scarce, but they are very instructive as they reveal the interplay between the electronic and nuclear structure during the dissociation process. Such studies are even more powerful when the double ionization mechanisms can be distinguished. The autoionization and direct photo-double ionization (PDI) of water and the dissociation dynamics of select dication states resulting in $H^+ + OH^+$ and $H^+ + H^+ + O$ were studied in great detail by Sann *et al.* [11] and Streeter *et al.* [12] as well as by Reedy and coworkers [13]. While none of these studies identified SOC in the dissociation dynamics, more recent investigations on deuterated water molecules (D_2O) showed that SOC plays an important role in the sequential dissociation leading to $D^+ + D^+ + O$ [14] and in the scarce $D^+ + O^+ + D$ reaction channel [10] upon direct PDI. In the latter fragmentation channel, which has been the subject of many past experimental studies [15–21], recent highly differential electron-ion coincidence experiments focused on the slow sequential breakup [10]. For this reaction, the role of super-excited states in the autoionization process in $D^+ + O^+ + D$ [22] was studied, and the branching ratios of electronically excited OD^+ transients to produce $D^+ + O^+ + D$ and $D^+ + D^+ + O$ [10] were measured. However, the SOC-enabled fast dynamics at the wells, seams, and parallel states of the water PESs near the Franck-Condon (FC) region is so far largely unexplored.

Hence, the present work is devoted to the state-selective investigation of the competition between the multi-step dissociation pathways of D_2O^{2+} dications near the FC region leading to the rare $D^+ + O^+ + D$ fragmentation channel after direct PDI by a single photon. With guidance from theory, we use the measured kinetic energies of the emitted electrons and the kinetic energy release (KER) of the dissociating water dications as observables to identify the electronic states involved and the required transitions between the states at play as well as the dissociation limits reached. Based on these results, this collaborative work between experiment and theory is able to identify and isolate the different conceivable ionization processes, fragmentation scenarios and their ultrafast dynamics (below 100 fs), and trace the spin-nonconserving transitions on wells, seams, and parallel states that were accessed during the dissociation process and eventually produced this rare breakup channel. The relative yields of the dissociation pathways can be extracted, which informs us about the efficiencies of SOC at these very transitions. Moreover, the measured particle momenta and angular distributions enable us to deduce the molecular geometries and orientations with respect to the polarization vector of the light as well as the ultrafast time scales of the dynamics at play.

II. EXPERIMENT

The experiments were performed at the undulator beamline 10.0.1.3 at the Advanced Light Source (ALS) synchrotron ring at the Lawrence Berkeley National Laboratory, and the experimental setup was similar to the one described in Refs. [10, 13]. Briefly, single linearly-polarized photons of 61 eV energy are absorbed in a well-localized interaction region ($\approx 1.0 \times 0.3 \times 0.3$ mm^3). This region is spanned by the adiabatically cooled D_2O gas jet target (≈ 50 K parallel and ≈ 15 K perpendicular to the jet propagation direction) and the monochromized light beam (with $\Delta E \approx 200$ meV) [23], which are intersected at right angles to each other inside the particle momentum spectrometer. Due to the inherent capability of the reaction microscope to mass-select fragment ions [24–26], several reaction channels can be distinguished [10, 13, 14]. Choosing D_2O as the target molecule enabled us to distinguish between PDI events from any residual H_2O background present in the vacuum chamber ($\approx 1.2 \times 10^{-8}$ Torr) and the supersonic gas jet. Moreover, the electric extraction field and spectrometer geometry were optimized to ensure that there was no overlap between the $D^+ + O^+ + D$ channel and the neighboring $OH^+ + D$ and $OD^+ + D^+$ two-body breakups in the PhotoIonPhotoIon COincidence (PIPICO) time-of-flight (TOF) spectrum (not shown here).

For the PDI of D_2O, resulting in the rare $D^+ + O^+ + D$ breakup channel, we measured two electrons (≤ 30 eV) and the ionic fragments (≤ 22 eV) in coincidence within the full 4π solid angle on their respective micro-channel plate (MCP) detectors, which were equipped with fast delay-line readouts [27, 28]. In contrast to the measured D^+ [$\Delta p(D^+) \approx 0.7$ a.u.] and O^+ ions [$\Delta p(O^+) \approx 1.9$ a.u.], the momentum of the neutral D particle [$\Delta p(D) \approx 2.3$ a.u.] was derived using momentum conservation for each event. From their momenta, we deduced the kinetic energies of the electrons ($\Delta E/E \approx 10\%$) and heavy fragments. The kinetic energy release of the dissociating water dications (ranging from 4 to 11 eV in this measurement with $\Delta KER/KER \leq 5\%$) and the relative angular distributions of the heavy fragments in the laboratory and molecular frames were investigated state-selectively.

III. OBSERVATION & ANALYSIS

Following the absorption of a single VUV photon, the D_2O molecule can either directly emit two electrons (direct PDI) or undergo subsequent expulsion of electrons by autoionization processes [10, 11, 13, 22]. In this investigation on the $D^+ + O^+ + D$ channel, we focus on the direct PDI (the autoionization is discussed elsewhere) [22]. After the emission of two electrons, the water dication can fragment directly into either two or three bodies [10, 13, 14]. In the $OD^+ + D^+$ two-body breakup, the hydroxyl ion can undergo a second fragmentation

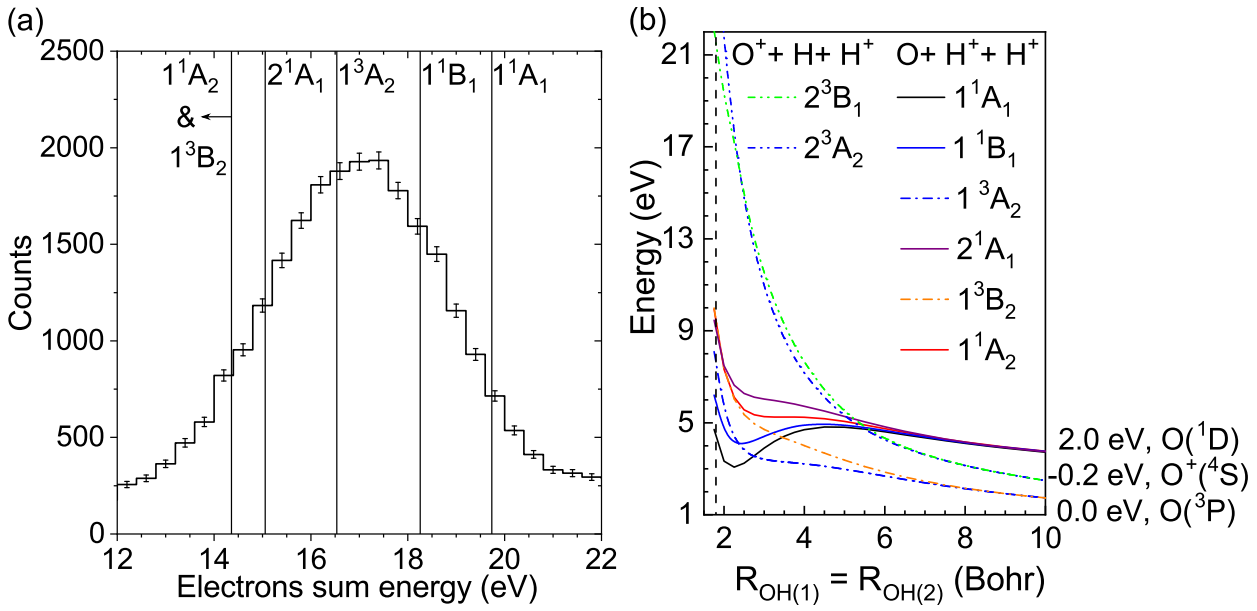

FIG. 1. (a) Measured photoelectron sum energy $E_{e_{sum}}$ distribution for the dication states leading to the $D^+ + O^+ + D$ fragmentation channel. The vertical lines indicate the expected $E_{e_{sum}}$ of the dication states at the equilibrium geometry of neutral water derived from PECs in panel (b). All error bars reflect one standard deviation in the statistical uncertainty. (b) PECs for the symmetric stretch of the H_2O^{2+} states dissociating into $H^+ + H^+ + O$ and $H^+ + O^+ + H$; from [12] and corrected by -0.77 eV (see text). The zero-energy value of the y-axis corresponds to the $H^+ + H^+ + O(^3P)$ dissociation limit with a PDI threshold of 36.7 eV [17]. The photon energy of 61 eV, therefore, corresponds to 24.3 eV on the ordinate.

step, yielding either $D^+ + O$ or $O^+ + D$ [10, 14]. This sequential fragmentation, along with the direct pathway, contributes to the formation of the rare $D^+ + O^+ + D$ reaction channel we investigate. Despite its rarity, the $D^+ + O^+ + D$ breakup channel could be identified and isolated with significant statistics for detailed analysis. The PDI yield branching ratios of these three fragmentation channels are 47.5% for $D^+ + OD^+$, 51.8% for $D^+ + D^+ + O$, and 0.7% for $D^+ + O^+ + D$ with a relative error of $\leq 1\%$ each. Note that the 47.5% for $D^+ + OD^+$ refers to the fraction that goes into long-lived rovibrational states of OD^+ and does not contribute to what is observed as a 3-body dissociation, while the 51.8% refers to the total fraction that fragments into $D^+ + D^+ + O$ either via direct or sequential breakup.

A. ELECTRONIC STATES, FRAGMENTATION PROCESSES, & MOLECULAR VIBRATIONS

For the $D^+ + O^+ + D$ reaction channel, the electron sum energy shown in Fig. 1(a) is peaked at 17 eV, corresponding to an *average* vertical ionization potential (VIP) of 44 eV. The measured electron sum energy distribution spans the potential energies of six valence excited states of the D_2O^{2+} dication, specifically the 1^1A_1, 1^1B_1, 1^3A_2, 1^3B_2, 2^1A_1, and 1^1A_2 states depicted in Fig. 1(b) that were previously shown to mainly dissociate to $D^+ + OD^+$ and $D^+ + D^+ + O$ [12]. Note that throughout this paper, to avoid confusion, we will label the various water dication states by their symmetric (C_{2v}) spectroscopic designations - A_1, A_2, B_1, and B_2, - with the understanding that for asymmetric geometries these should be replaced by their C_s designations - A′, A″, A″, and A′, respectively.

In the present work, we make several comparisons between H_2O and D_2O, which have identical electronic states, but different vibrational structure. We also expect different fragment momenta (scaling with $\sqrt{m}$), however, the energies of the dissociative states and three-body dissociation limits are identical. For most, if not all, aspects of the present work the fragmentation dynamics of the two isotopologues are directly comparable. The calculations of Streeter *et al.* [12] report PECs of the water dication that feed the fragmentation channels $H^+ + O^+ + H$ and $H^+ + H^+ + O$ via symmetric stretch of both OH bonds. In the present work, the energy scale of those PECs was shifted by -0.77 eV to agree with the well-known thermodynamic value of the $H^+ + H^+ + O(^3P)$ asymptote. The relevant adjusted PECs and dissociation limits are shown in Fig. 1(b). The measured total kinetic energy in our experiment, i.e., the sum of the KER and the electron sum energy after PDI of D_2O with 61 eV photons, is very close to the $D^+ + D^+ + O(^3P)$ asymptote (see Fig. 2 in Ref. [10]) and leads us to conclude that the D_2O^{2+} dication dissociates to the $D^+ + O^+(^4S) + D$ limit, which is known to be very close to the $D^+ + D^+ + O(^3P)$ limit (i.e.,

within $\sim$ 0.02 eV, based on spectroscopic data). Note that the calculations of Streeter *et al.* in Ref. [12] incorrectly place the $H^+ + H^+ + O$ asymptote 0.2 eV above the $H^+ + O^+ + H$ limit, an error related to the difficulty of calculating the ionization potential (IP) of atomic oxygen (13.618 eV) relative to that of hydrogen (13.598 eV). This will be addressed further below.

In the FC region [centered around the dashed vertical line in Fig. 1(b)], the potential energies of the D_2O^{2+} states that are leading directly to $D^+ + O^+ + D$ are located at a VIP of approximately $21 + 36.7 = 57.7$ eV, i.e., 13.7 eV higher than the observed average VIP of 44 eV, deduced from the electron sum energy, which is displayed in Fig. 1(a). This prompts us to conclude that the fragmentation occurs via a multi-step dissociation process in which the $D^+ + O^+ + D$ fragmentation channel can only be reached in a path that involves a sequence of non-adiabatic couplings of PESs, each leading to either $D_2^+ + O^+$, $D^+ + D^+ + O$, or to $D^+ + OD^+$ as intermediate reaction products. In contrast to the lower valence dication states of water [29], PESs for the asymmetric stretch of D_2O^{2+}, leading directly to $D^+ + O^+ + D$, are not yet available. Nevertheless, as we have verified through *ab initio* calculations, even large changes of the geometry in or close to the FC region to lower the potential energy of the lowest relevant repulsive dication states, 2^3B_1 or 2^3A_2, by 13.7 eV, are highly unlikely.

Similarly, the bond rearrangement and the formation of a stable D_2^+ ($1s\sigma_g$) cation during the first breakup step $D_2^+ + O^+$ at the equilibrium geometry of the water molecule, corresponding to an internuclear distance of $R \approx 3$ bohr between the deuteron and the deuterium atom, is expected to reside approximately 2 eV below the PEC for the direct production of $D^+ + O^+ + D$ for this value of R. According to the electron sum energy in Fig. 1(a), it is, hence, energetically inaccessible in our experiment. We therefore exclude the fragmentation process via the $D_2^+ + O^+$ intermediates as a potential first step in the sequential dissociation pathway of the D_2O^{2+} dication at 61 eV. This leaves us with the formation of either $D^+ + D^+ + O$ or $D^+ + OD^+$ as intermediate reaction pathways.

In our recent publication [10], we have applied the native frame analysis [30] to the $D^+ + O^+ + D$ breakup channel. We demonstrated that a slow sequential breakup of the D_2O^{2+} dication via the formation of excited OD^+ transients, which live longer than their rotational period, fragment with low KER of the OD^+ dissociation (denoted KER_{OD} hereafter) and finally produce the rare $D^+ + O^+ + D$ channel. After the breakup of D_2O^{2+} into $D^+ + OD^+$ in the first step, the dissociation of the transient OD^+ in the second step requires multiple SOCs to reach the $O^+(^4S) + D$ limit. We were able to divide the data into two parts, using the kinetic energy release of the second breakup step, KER_{OD}, and the angle, $\theta_{OD,D}$, between the conjugate momenta of the first and second dissociation steps (see Fig. 4 in Ref. [10]). We found that for $KER_{OD} \leq 0.25$ eV, the angular distribution in $\theta_{OD,D}$ is mostly flat, which is a signature of a slow sequential breakup via an OD^+ intermediate that rotates long enough in the fragmentation plane to yield a nearly uniform angular distribution (see Ref. [10]). The rest of the data related to $KER_{OD} > 0.25$ eV does not lead to a uniform angular distribution $\theta_{OD,D}$, which indicates that any possible OD^+ intermediate dissociates faster than the rotational period of OD^+, i.e., before one full rotation was completed. These fast dissociation scenarios that are related to $KER_{OD} > 0.25$ eV, were not investigated in Ref. [10], but they are the focus of our study in this manuscript. The relative yields of the high-KER_{OD} ($KER_{OD} > 0.25$ eV) and low-KER_{OD} ($KER_{OD} \leq 0.25$ eV) contributions for the direct PDI of D_2O, resulting in the $D^+ + O^+ + D$ channel, are 53.2% $\pm$ 5% and 46.8% $\pm$ 5%, respectively.

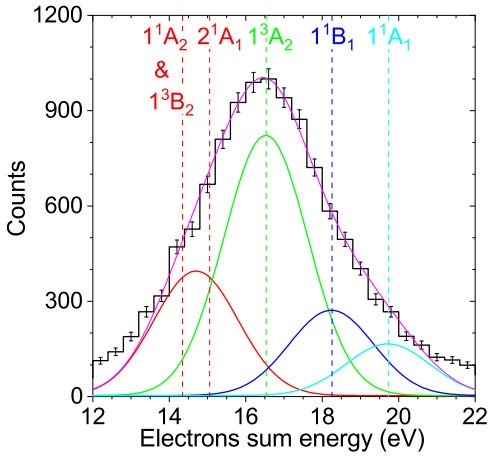

FIG. 2. Measured electron sum energy E_{esum} for the dication states leading to high-KER_{OD} (> 0.25 eV) of the $D^+ + O^+ + D$ fragmentation channel (black line). The vertical lines indicate the energies of the dication states. Four Gaussians are fitted to the data. The first Gaussian fit (red line) represents the 1^3B_2, 2^1A_1, and 1^1A_2 dication states (23.9% $\pm$ 0.5%), the second Gaussian fit (green line) represents the 1^3A_2 dication state (49.9% $\pm$ 0.6%), the third Gaussian fit (blue line) represents the 1^1B_1 dication state (16.3% $\pm$ 0.7%), and the fourth Gaussian fit (cyan line) represents the 1^1A_1 dication state (9.9% $\pm$ 0.5%). The sum of all four Gaussians is represented by the magenta line. All error bars reflect one standard deviation in the statistical uncertainty.

The associated electron sum energy E_{esum} distribution of these high-KER_{OD} events, which is peaked at 16.5 eV, is presented in Fig. 2. In contrast to the data depicted in Fig. 1(a), Fig. 2 only shows data for which KER_{OD} exceeds 0.25 eV. A multi-Gaussian fit to this electron sum energy distribution, based on the expected vertical energies of the dication states depicted in Fig. 1(b), is also shown. The distribution is well-represented by four Gaussian functions (using only three Gaussians resulted in a poorer fit). The Gaussian width, determined by fitting the electron sum energy distribution for the

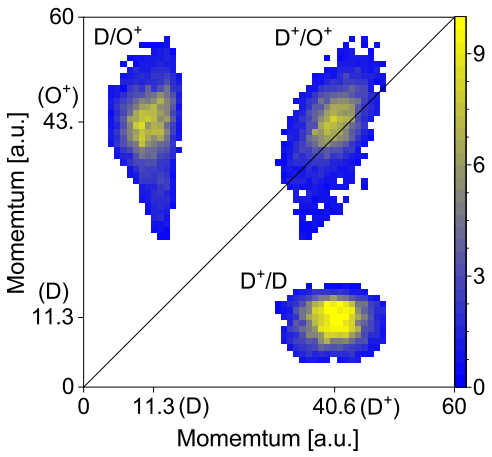

FIG. 3. Lab frame fragment momentum correlation diagram: Yield attributed to the 1^3B_2, 1^1A_2, 2^1A_1, 1^3A_2, 1^1B_1, and 1^1A_1 dication states of water after PDI at 61 eV resulting in $D^+ + O^+(^4S) + D$ with high-KER_{OD} as a function of the momenta of the fragment pairs D^+/D, D^+/O^+, and D/O^+: see labels at axes and islands. The average momenta of the nuclear fragments are indicated on the x- and y-axes.

dominating direct three-body channel $D^+ + D^+ + O$ (not shown), exhibits minimal variation (less than 10% disparity) across the contributing dication states. Therefore, a single width value is used for all four Gaussians in the fits. In particular the 1^3A_2 dication state dominates with 49.9% ± 0.6%, while the 1^1B_1 and 1^1A_1 dication states account for 16.3% ± 0.7% and 9.9% ± 0.5%, respectively. The 1^3B_2, 1^1A_2, and 2^1A_1 dication states contribute at around 23.9% ± 0.5%. Note that our resolution does not allow us to distinguish between the 1^3B_2, 1^1A_2, and 2^1A_1 dication states. In contrast to the high-KER_{OD} events, the low-KER_{OD} contribution ($KER_{OD} \leq 0.25$ eV), investigated in Ref. [10], showed a dominance of the 1^1B_1 dication state with 55.4% ± 0.8%, while the 1^3A_2 and 2^1A_1 states contributed almost equally at 24.2% ± 1.2% and 20.4% ± 1%, respectively.

B. DISSOCIATION PATHWAYS IN THE LABORATORY & MOLECULAR FRAME

The only dication states that can dissociate directly to $D^+ + O^+(^4S) + D$ following PDI of D_2O are the 2^3A_2 and 2^3B_1 states, which, according to our measured KER and correlated $E_{e_{sum}}$, are not directly populated in the FC region by a 61 eV photon. We now present the most likely state-selective, multi-step processes needed to produce the detected $D^+ + O^+(^4S) + D$ channel, firstly via symmetric stretch (Sec. III B 1) and then via small (Sec. III B 2) and large (Sec. III B 3) asymmetric stretch of D_2O^{2+}. We concentrate herein on fragmentation scenarios that require only one SOC transition, since conceivable multi-step processes with several SOCs are expected to be very inefficient.

1. SOC enabled direct breakup following symmetric stretch

The 1^3A_2 and 1^3B_2 dication states, both leading to the $D^+ + D^+ + O(^3P)$ dissociation limit, lie only 0.02 eV below the $D^+ + O^+(^4S) + D$ asymptote. From the extended PECs of the 1^3A_2 and 1^3B_2 dication states [see Fig. 1(b)] beyond 10 bohr, we expect their crossings with the $D^+ + O^+(^4S) + D$ PECs to occur at distances R > 20 bohr. For two-body interactions at such large distances, we anticipate the D^+ and D fragments to yield very similar momenta, which is not the case for these high-KER_{OD} events. The momentum correlation map of the three heavy fragments in the lab frame, shown in Fig. 3 for the high-KER_{OD} contribution, reveals that the momentum of the neutral D fragment is ≈ 4 times lower than that of the D^+. Therefore, a scenario in which the 1^3A_2 and 1^3B_2 dication states dissociate into $D^+ + D^+ + O(^3P)$ in the first step of the fragmentation process before a subsequent charge exchange takes place can be removed from consideration.

We now turn our attention to the singlet dication states 1^1A_1, 1^1B_1, 1^1A_2, and 2^1A_1. According to the PECs in Fig. 1(b), presented in C_{2v} geometry, these states cross the 2^3A_2 and 2^3B_1 dication states between 5.0 and 6.0 bohr. If SOC transitions to the latter states take place, they will lead to the detected final products $D^+ + O^+(^4S) + D$. However, with first-row molecules, in the absence of potential wells in the metastable electronic states, isolated crossings between singlet and triplet states are rather inefficient in facilitating such charge-exchange. This is not necessarily true for states that form wells or run flat or in parallel at intermediate geometries or asymptotically, as we will consider below. From these four dication states only the 1^1A_1 and 1^1B_1 states exhibit very shallow wells in the crossing region. A vertical excitation to the 1^1B_1 state produces the water dication just above the dissociation barrier, while a vertical transition to the 1^1A_1 does not surpass this threshold. However, it is conceivable that the population of 1^1A_1 vibration levels close to the barrier top can get trapped in a similar fashion as the 1^1B_1 state and allow for some SOC transitions to take place.

To further assess this dissociation scenario for the 1^1A_1 and 1^1B_1 dication states, we now investigate the distributions of relative angles between the heavy fragments. While integrating over the direction of the polarization vector of the incoming light, we define the molecular breakup frame via the measured momentum vectors of the three heavy fragments in the laboratory frame, which establish a fragmentation plane. Azimuthal relative angles $\phi_{A,B}$ between the momenta of fragments A and B are measured around the normal of this plane. The azimuthal angle $\phi_{D^+,D}$ between the measured momenta of the D^+ ion and the neutral D fragment in the molecular fragmentation frame is shown in Fig. 4 (red line). This relative angle $\phi_{D^+,D}$ exhibits a rather broad distribution peaked at ≈ 88°, which is appreciably smaller than the

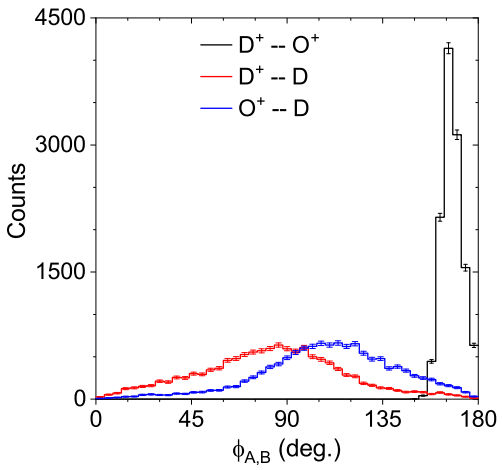

FIG. 4. Relative angles $\phi_{A,B}$ in the molecular breakup plane of D_2O^{2+} between fragment pairs D^+ and O^+ (black), D^+ and D (red), and O^+ and D (blue) for the high-KER_{OD} feature (1^3B_2, 1^1A_2, 2^1A_1, 1^3A_2, 1^1B_1, and 1^1A_1 dication states). All error bars represent one standard deviation in the statistical uncertainty. Note that only two of the relative angles are independent observables.

bond angle of the neutral water molecule (104.5°). Our momentum uncertainty is contributing to a large degree to the broad shape of the $\phi_{D^+,D}$ and $\phi_{O^+,D}$ distributions. However, for this high-KER_{OD} feature, the peak positions are rather unaffected by the resolution (see discussion in [10]). The relative angle resolutions of $\phi_{D^+,D}$ and $\phi_{O^+,D}$ are expected to be on the order of 22° and 24°, respectively.

We now correlate the dissociation angles with the potential energies. Around the FC region, the 1^1B_1 dication state exhibits a strong gradient towards bond opening, i.e., an increase in the DOD angle during the dissociation, and the 1^1A_1 state stays rather flat [12]. Once the bonds stretch symmetrically and crossings to the 2^3A_2 and 2^3B_1 dication states occur via SOC followed by charge localization on the atomic centers, the newly formed neutral D fragment will keep its emission direction without being further affected by the charged fragments. The Coulomb repulsion between the D^+ and the O^+ ions experienced in the second step will decrease their respective relative angles with the neutral D fragment, i.e., $\phi_{D^+,D}$ and $\phi_{O^+,D}$ will get smaller. The observed peak of $\phi_{D^+,D}$ at $\approx 88°$ in Fig. 4 (red line), which is around 16.5° lower than the bond angle of the neutral water molecule (104.5°), might be an indicator of the changing Coulomb field in the transition from the intermediate $D^+ + D^+ + O$ to the final $D^+ + O^+ + D$ reaction products during the dissociation process in which the O is oxidized.

Based on the PECs of the 1^1A_1 and 1^1B_1 dication states and their crossings with the 2^3A_2 and 2^3B_1 dication states, which mark the endpoints for this dissociation step, we classically estimate the time from the double ionization to the SOC to be less than 60 fs.

We can summarize this dissociation scenario following direct double ionization of D_2O resulting in high-KER_{OD} and proceeding via the intermediates 1^1A_1 and 1^1B_1 dication states while involving symmetric stretch of D_2O^{2+} as:

SCENARIO (I): SOC enabled direct breakup following symmetric stretch

1) $D_2O^{2+}(1^1A_1, 1^1B_1) \xrightarrow{\text{sym. stretch}}$
2) $D_2O^{2+}(1^1A_1, 1^1B_1)_{(D^+ + O(^1D) + D^+\ limit)} \xrightarrow{\text{SOC}}$
3) $D_2O^{2+}(2^3A_2, 2^3B_1)_{(D^+ + O^+(^4S) + D\ limit)} \xrightarrow{frag.}$
4) $D^+ + O^+(^4S) + D$

2. SOC enabled direct breakup following small asymmetric stretch

To further assess the role of the singlet dication states, a small asymmetric stretch is introduced to the dissociating molecule. We examined the 1^1A_2, 2^1A_1, 1^1B_1 dication states near HOH angles of 85° and various asymmetric bond lengths. We also examined the 2^3A_2 state at the same geometries. The results are depicted in Fig. 5. Since the 2^3A_2 state was not considered in either Ref. [12] nor Ref. [29], the data shown in Fig. 5 was calculated from complete-active space (CAS) plus singles and doubles multi-reference configuration-interaction (MRCI) calculations with state-averaged natural orbitals. The oxygen 1s orbital was held doubly occupied and seven orbitals were included in the active space. The selection of 85° HOH angles is justified by the observed $\phi_{D^+,D}$ angle peaking at $\approx 88°$ in Fig. 4 (red line). Throughout the remaining discussion, we distinguish the first and second D fragments in a dissociation process that involves asymmetric stretch by indices (I) and (II), respectively. In Fig. 5 we see that for different short O-H_{II} bond lengths, fixed at 4.5, 4.6, and 4.9 bohr for the 2^1A_1, 1^1A_2, and 1^1B_1 dication states, respectively, the singlet states approach the 2^3A_2 state in energy over a continuous range of long O-H_I distances between 5 and 6 bohr. There are clearly seams of intersections in this region extending over several bohr where the singlet states, which are linked to the $D^+ + D^+ + O$ dissociation limit, and the triplet state, which is linked to the $D^+ + O^+ + D$ limit, are degenerate, making a spin-orbit charge exchange possible.

However, these seams of degeneracy for the 1^1A_2, 2^1A_1, and 1^1B_1 dication states only provide evidence for this mechanism if the region where charge exchange is occurring can be reached energetically from the initial dication geometry. For that purpose, we have examined PESs of the relevant singlet dication states with a fixed asymmetric stretch of $R_{(2)} = R_{(1)}$ - 1 bohr (see Fig. 6), using the analytic fits to the *ab initio* surfaces given by Gervais et al. [29] to generate the plots in Fig. 6. $R_{(1)}$ and $R_{(2)}$ refer to the bond distances between the O and the H_I particle and the other H_{II} fragment, respectively.

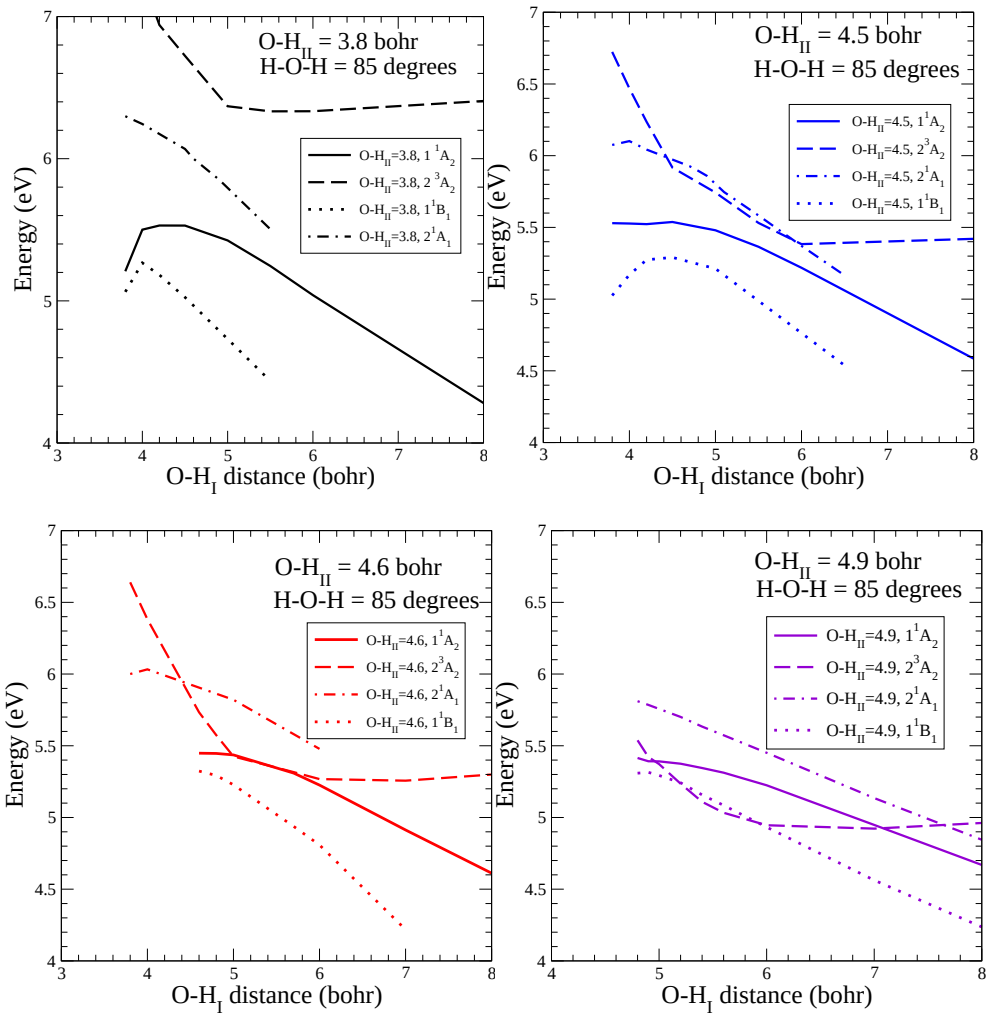

FIG. 5. Calculated cuts through the PESs of the 1^1A_2, 2^1A_1, 1^1B_1, and 2^3A_2 dication states at fixed HOH-bond angles of 85° for a range of asymmetric geometries with the O-H_{II} stretch being fixed (see insets) while the O-H_I stretch is varied. The electron transfer is happening between the O and the more distant singly-charged H_I, while H_{II} remains singly-charged.

The selection of $R_{(2)} = R_{(1)}$ - 1 bohr is justified by the bond lengths at the seams of intersections, as shown in Fig. 5. As the PECs reveal, near the geometry of neutral water molecules, the energies of the 1^1B_1 and 2^1A_1 dication states are lowered with increasing HOH bond angle, while that of the 1^1A_2 state favors a decrease in bond angle, and the potential energy for the 1^1A_1 dication state stays rather flat (see Fig. 5 in Ref. [12]). However, for OH distances greater than ≈ 3.5 bohr, the energies of all four singlet states drop with increasing angle, since the energy is determined mostly by the Coulomb repulsion between the two protons rather than by their bonding to the oxygen. From the equilibrium geometry of the neutral water to the region around the seam of intersection, the examination of the PES for the 1^1A_2 and 2^1A_1 dication states in Fig. 6 shows that a path from 104.5° to 85° is energetically downhill and thus favorable. In contrast, for the 1^1B_1 dication state in Fig. 6 the path from 104.5° to the plateau region near 85° is energetically uphill. A similar situation is apparent for the 1^1A_1 state, where we find barriers (not shown here) which prevent a path to the plateau region where seams of degeneracy could be formed. This leaves only the 1^1A_2 and 2^1A_1 states as candidates for this dissociation scenario.

To assess the relative contributions of the 1^1A_2 and 2^1A_1 states as candidates for SOC charge exchange with the 2^3A_2 dication state, we must examine the wavefunctions of the dications in the region where the PESs intersect, i.e., where both O-D separations lie between 4 and 6 bohr. At those geometries, the wavefunctions for the three water dication states in question can be approximated as contributions from the following orbitals:

1^1A_2: $3a_1^2\ 1b_1\ 1b_2$
2^1A_1: $3a_1^0\ 1b_1^2\ 1b_2^2$
2^3A_2: $3a_1\ 1b_1\ 1b_2\ 4a_1$,

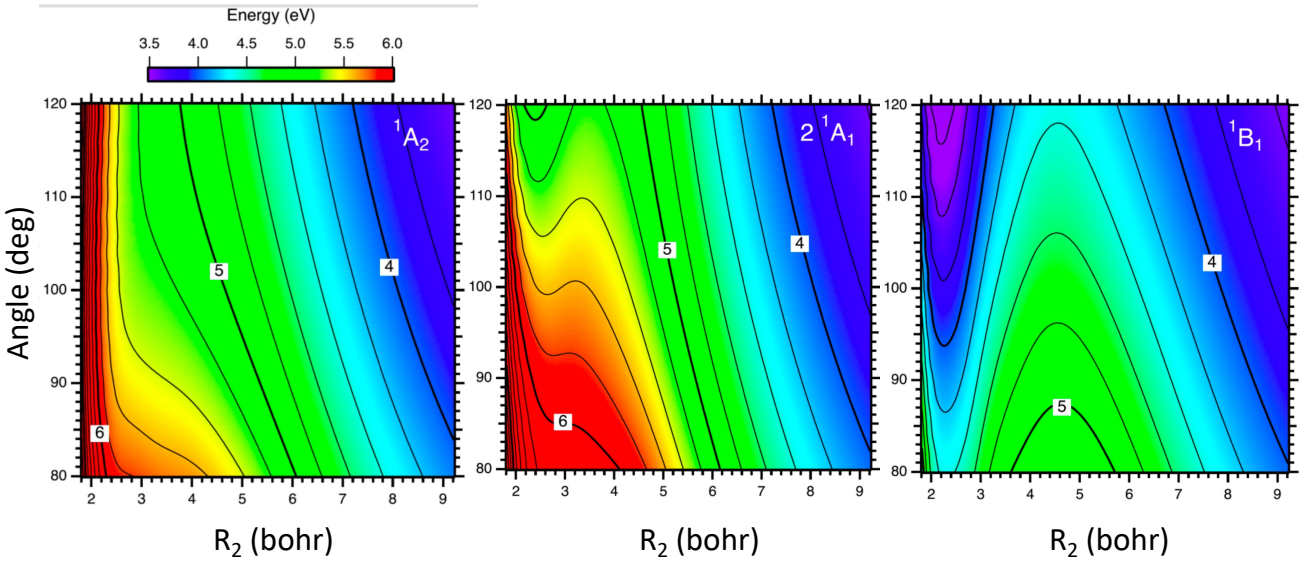

FIG. 6. PESs derived from analytical fits to the *ab initio* data from Ref. [29] for the (left) 1^1A_2, (middle) 2^1A_1, and (right) 1^1B_1 water dication states as a function of specific asymmetric OD_I and OD_{II} bond distances and the DOD bond angle. $R_{(1)}$ refers to the first-emitted D_I particle, while $R_{(2)}$ refers to the other D_{II} fragment. The plotted energies for all three states are a function of the fixed small asymmetric stretch $R_{(2)} = R_{(1)}$ - 1.0 bohr. The energy contour lines, relative to the $O(^3P) + D^+ + D^+$ dissociation limit, are spaced 0.2 eV apart. The same color-energy scale is used for all three states.

where $3a_1$, $1b_1$, and $1b_2$ are basically oxygen-centered (s+z), x, and y orbitals, respectively, and $4a_1$ is a deuterium-centered 1s orbital. Consequently the SO matrix elements look like:

$$<1^1A_2|H^{SO}|2^3A_2> = <3a_1|H^{SO}|4a_1>$$
$$<2^1A_1|H^{SO}|2^3A_2> = <1b_1 1b_2|H^{SO}|3a_1 4a_1>.$$

Armed with these approximations, we see that the first expression, $<1^1A_2|H^{SO}|2^3A_2>$, is a simple one-body matrix element and therefore much larger than the second one, $<2^1A_1|H^{SO}|2^3A_2>$, which is a two-electron spin-other orbit matrix element involving a double excitation [2]. This leaves only the 1^1A_2 dication state as a probable contributor to the $D^+ + O^+(^4S) + D$ production in this protracted direct breakup scenario, which is proceeding via a small asymmetric stretch on seams formed at intermediate internuclear distances that efficiently support SOC.

We summarize this dissociation scenario following the direct double ionization of water after small asymmetric stretch proceeding via the intermediate 1^1A_2 dication state resulting in high-KER$_{OD}$, which can be seen as a variant of scenario (I), as:

SCENARIO (II): SOC enabled direct breakup following small asym. stretch

1) $D_2O^{2+}(1^1A_2) \xrightarrow{\text{small asym. stretch}}$
2) $D_2O^{2+}(1^1A_2)_{(D_I^+ + OD_{II}^+(1^1\Pi)\ limit)} \xrightarrow{\text{SOC}}$
3) $D_2O^{2+}(2^3A_2)_{(D_I + O^+(^4S) + D_{II}^+\ limit)} \xrightarrow{frag.}$
4) $D_I + O^+(^4S) + D_{II}^+$

3. SOC and charge exchange during fast sequential breakup

We have yet to account for $D^+ + O^+(^4S) + D$ production via the 1^3A_2 or 1^3B_2 dication states. The 1^3A_2 state in particular appears to be a major contributor, based on the measured and fitted $D^+ + O^+(^4S) + D$ yields as a function of the photoelectron sum energy [see Fig. 2]. Both states show no crossings with the 2^3A_2 or 2^3B_1 dication states in C_{2v} geometry at intermediate O-D separations and dissociate predominately via direct 3-body breakup to $O(^3P) + 2D^+$ [see Fig. 1(b) and Refs. [12, 29]]. In the 2-body limit, they correlate with the production of D^+ plus the two components of $OD^+(A^3\Pi)$.

We now present a detailed investigation of the latter two-body breakup option as a potential intermediate dissociation route for the 1^3A_2 and 1^3B_2 dication states. Based on the calculations of Gervais *et al.* (see Fig. 2 in Ref. [29]), it is conceivable that a sequential breakup can be initiated at asymmetric (C_s) geometries of D_2O^{2+}, aiming towards a fast ejection of D_I^+ from D_2O^{2+} into $D_I^+ + OD_{II}^+$ and a simultaneous slower separation of OD_{II}^+ within which a charge-exchange transition to $O^+ + D_{II}$ takes place. As noted in Sec. III A, the intermediate OD_{II}^+ dissociates faster than the rotational period of OD_{II}^+ (the latter is estimated to be about 1 ps, using the rigid rotor approximation for OD^+ at $R_{O-D} = 2$ a.u. and j = 1). Accordingly, we call this fragmentation route "fast sequential breakup".

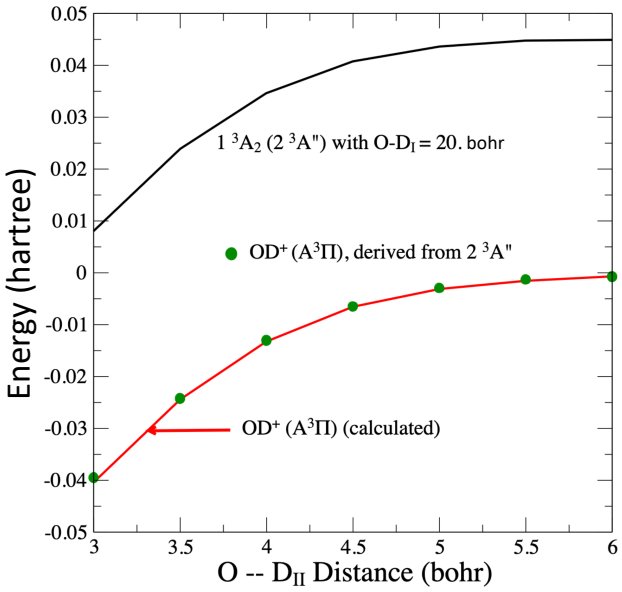

FIG. 7. OD$^+$(A$^3\Pi$) PEC derived from the D_2O^{2+}(1^{3}A$_2$) dication state. The derived energy values (green solid circles) were obtained by subtracting the Coulomb repulsion energy between the two D^+ ions from the 1^{3}A$_2$ dication energy (black line). The derived points are plotted along with the computed OD$^+$(A$^3\Pi$) PEC (red line).

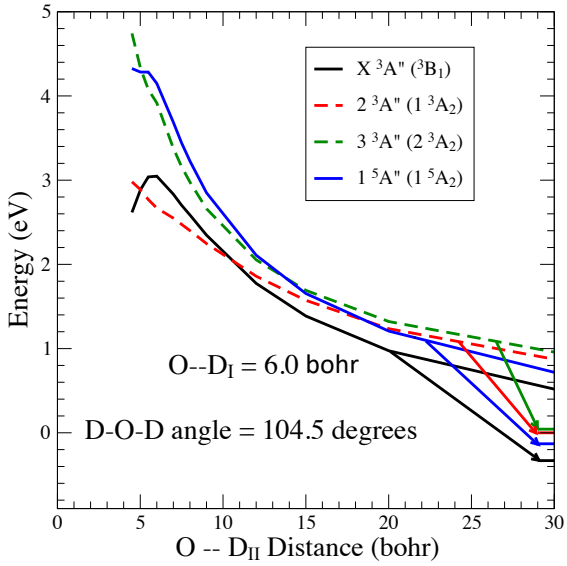

FIG. 8. Selected D_2O^{2+} PECs for asymmetric stretch. The D-O-D angle is fixed at 104.5°; the X^{3}B$_1$ and 1^{5}A$_2$ dication states are shifted up by 0.5 eV to correct for the asymptotic error (see text).

To approach this two-body breakup option computationally, a question that must be asked is: how far must the D^+ ion be from the OD^+ fragment before it can be treated as a spectator? Or in other words: at what separation between ionic D_I^+ and OD_{II}^+ fragments can the electronic energy of the dication be well-approximated by the sum of the OD_{II}^+ energy and the Coulomb repulsion between OD_{II}^+ and D_I^+? This question is answered by the results shown in Fig. 7, where we compare the calculated PEC of OD_{II}^+(A$^3\Pi$) (red line) with values derived by subtracting the Coulomb repulsion energy $1/|R(D_{II}^+) - R(D_I^+)|$ from the calculated 1^{3}A$_2$ water dication energy (black line). This difference is represented by the solid green circles, and it is in very good agreement with the calculated PEC of OD_{II}^+(A$^3\Pi$). We note that virtually identical results were obtained for the 1^{3}B$_2$ state. The 1^{3}A$_2$ and 1^{3}B$_2$ dication states correlate with the two degenerate PEC components of the $D_I^+ + OD_{II}^+$(A$^3\Pi$) dissociation. These calculations were carried out for an O-D$_I$ separation of 20 bohr, but similar results were also obtained with an O-D$_I$ separation as small as 9 bohr.

Another feature of the water dication that must be addressed is the fact that virtually all *ab initio* calculations, including this one, incorrectly place the asymptotes of the states that dissociate to O(^{3}P) + 2D$^+$ above those that dissociate to $D^+ + O^+(^4S) + D$, when in fact they are nearly degenerate. This error stems from the difficulty of calculating the relative IPs of atomic oxygen (which is challenging) and atomic hydrogen (which is easy). In the present context, in which the dissociation mechanism involves a transition at large O-D separations, we compensate for the asymptotic error by shifting the relevant $O^+ + D$ curves upward by 0.5 eV to insure the proper asymptotic splittings.

With these adjustments in place, we are now in a position to propose a dissociation mechanism for the 1^{3}A$_2$ and 1^{3}B$_2$ water dication states. Fig. 8 shows several water dication PECs at a fixed D-O-D angle, where one O-D distance is fixed at 6.0 bohr and the other O-D separation is varied. We note that for O-D$_{II}$ distances greater than ≈ 7 bohr, the 1^{3}A$_2$ and X^{3}B$_1$ dication states are energetically close. At those distances, the X state can be populated by essentially an atomic spin-orbit coupling on oxygen, which does not involve a charge-exchange and is largely R-independent. At larger separations, for which the fast D_I^+ ion has moved on, we only need to look at the diatomic OD_{II}^+ PECs (see Fig. 7) to track the dynamics. The OD_{II}^+ states are plotted in Fig. 9.

Looking at Fig. 9, one would expect competing A$^3\Pi \rightarrow$ 1$^5\Sigma^-$ and A$^3\Pi \rightarrow$ B$^3\Sigma^-$ transitions to take place in the dissociating OD_{II}^+ transient. Yet, the A$^3\Pi$ and 1$^5\Sigma^-$ states, which differ in both spin and symmetry, can only interact through second-order SOC and were thus excluded from consideration. A non-adiabatic transition between the A$^3\Pi$ and B$^3\Sigma^-$ states is facilitated by a matrix element describing the electronic orbital angular momentum coupling. The matrix element falls off as $1/R^2$. But since this angular coupling derives from the nuclear kinetic energy, it enters the Hamiltonian with a factor of one over the reduced mass ($1/\mu_{OD} = 1/3264$ a.u.) and is, hence, very small. Consequently, we single out the A$^3\Pi \rightarrow$ X$^3\Sigma^-$ transition as the dominant one.

The OD_{II}^+ states to which the 1^{3}A$_2$ and X^{3}B$_1$ dication

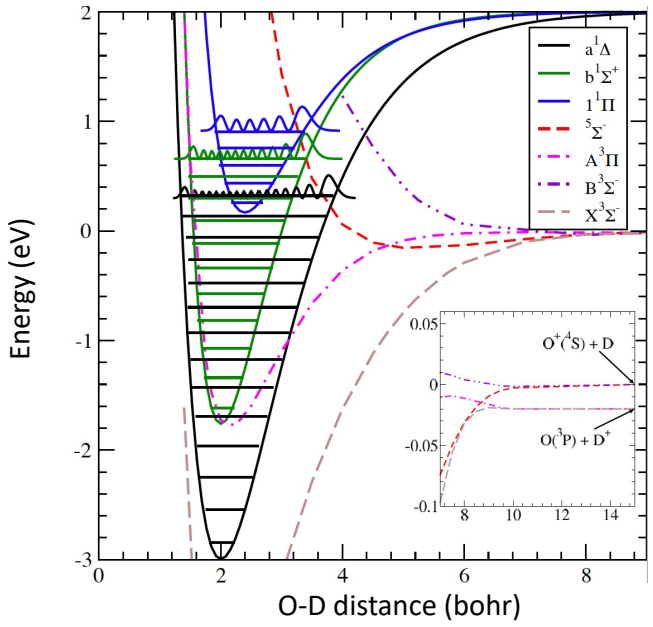

FIG. 9. Selected OD^+_{II} PECs. The vibrational levels of the $a^1\Delta$, $b^1\Sigma^+$, and $1^1\Pi$ cation states are shown, as well as the PECs of the $^5\Sigma^-$, $A^3\Pi$, $X^3\Sigma^-$, and $B^3\Sigma^-$ states. The dissociative limits of the latter four states are shown in the inset. The $a^1\Delta$, $b^1\Sigma^+$, and $1^1\Pi$ states all dissociate to $O(^1D_2) + D^+_{II}$, 1.95 eV above the $O^+(^4S) + D_{II}$ asymptote. The zero of energy is taken to be the $O^+(^4S) + D_{II}$ asymptote.

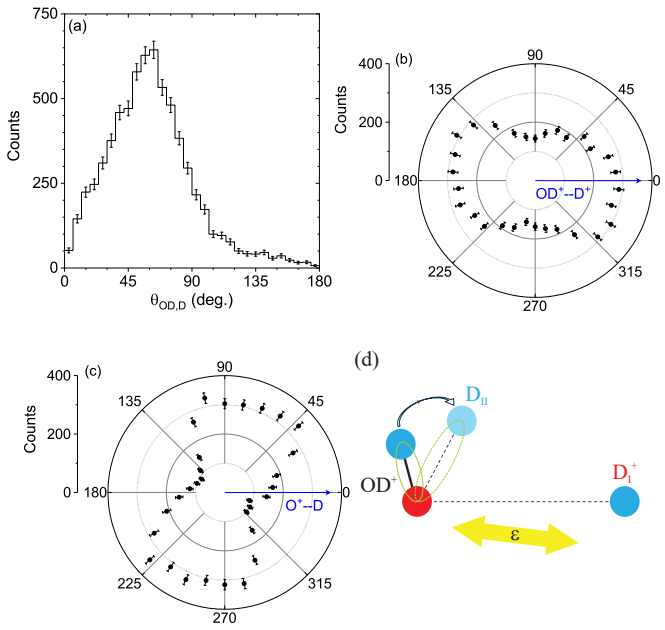

FIG. 10. Native frame analysis for the high-KER_{OD} contribution of the dissociating water dication leading to $D^+ + O^+(^4S) + D$ according to scenario (III) for the polarization vector being in the molecular plane (± 40°): (a) Relative angle $\theta_{OD,D}$ between the two fragmentation vectors (as defined in the text), (b) relative angular distribution of the polarization vector with respect to the first fragmentation axis $OD^+_{II} - D^+_I$ (P_{OD_{II},D_I} points to the right and $P_{OD_{II}}$ goes in the upper half), and (c) relative angular distribution of the polarization vector with respect to the second fragmentation axis $O^+ - D_{II}$ ($P_{OD_{II}}$ points to the right and P_{OD_{II},D_I} goes in the upper half). All error bars represent one standard deviation in the statistical uncertainty. The most probable orientation of the water molecule for an in-plane direct photo-double ionization in scenario (III), as discussed in the text, is sketched in panel (d). The polarization vector ϵ is represented by the tilted (yellow) double arrow (see text).

states correlate in the 2-body $D^+_I + OD^+_{II}$ limit are $A^3\Pi$ and $X^3\Sigma^-$, connected by an atomic oxygen SOC splitting, whose PECs begin to flatten at distances greater than ≈ 6 bohr. At these OD^+_{II} separations, the $X^3\Sigma^-$ and $B^3\Sigma^-$ states are also close. Note that the $B^3\Sigma^-$ and the $1^5\Sigma^-$ states are the only OD^+_{II} states that dissociate to $O^+(^4S) + D_{II}$. A non-adiabatic transition between $X^3\Sigma^-$ and $B^3\Sigma^-$ can then lead to $O^+ + D_{II}$. Incidentally, the dynamics just described also applies to the 1^3B_2 state. The fact that 1^3A_2 and 1^3B_2 do not contribute equally to the O^+ production (see Fig. 2) is no doubt related to their different vertical IPs in the FC region of about 2 eV and correspondingly different PDI cross sections at 61 eV photon energy.

To investigate this proposed dissociation scenario further, we conducted a native frame analysis [30] of our measured data. For D_2O^{2+} fragmenting into $D^+_I + O^+ + D_{II}$ via the intermediates $D^+_I + OD^+_{II}$, followed by the dissociation of OD^+_{II} into $O^+ + D_{II}$, the conjugated momentum vectors of the Jacobi coordinates associated with the relative motion of the fragments are calculated as follows: For the 1^{st} breakup step the relative momentum $P_{OD^+_{II},D^+_I}$ associated with the motion of the D^+ fragment relative to the center of mass of the OD^+ ion is given by

$$\mathbf{p}_{\mathrm{OD}^+_{II},\mathrm{D}^+_I} = \frac{m_{\mathrm{OD}}}{M}\mathbf{P}_{\mathrm{D}^+_I} - \frac{m_{\mathrm{D}}}{M}\left[\mathbf{P}_{\mathrm{D}_{II}} + \mathbf{P}_{\mathrm{O}^+}\right] = \mathbf{P}_{\mathrm{D}^+_I}, \quad (1)$$

where the last step in the above equation is a consequence of momentum conservation. For the 2^{nd} breakup step, related to the relative momentum $P_{OD^+_{II}}$ of the $O^+ + D$ motion, we get

$$\mathbf{p}_{\mathrm{OD}^+_{II}} = \mu_{\mathrm{OD}}\left[\frac{\mathbf{P}_{\mathrm{D}_{II}}}{m_{\mathrm{D}}} - \frac{\mathbf{P}_{\mathrm{O}^+}}{m_{\mathrm{O}}}\right], \quad (2)$$

where $\mathbf{P}_{\mathrm{D}^+_I}$ and $\mathbf{P}_{\mathrm{O}^+}$ are the measured momenta of the D^+ and O^+ fragments, respectively, while $\mathbf{P}_{\mathrm{D}_{II}}$ is the momentum of the neutral D fragment, which is derived from momentum conservation. Here m_{D} is the mass of D^+ or D, m_{OD} is the mass of OD^+, M is the mass of the D_2O^{2+} dication, and μ_{OD} is the reduced mass of OD^+.

The angle $\theta_{\mathrm{OD,D}}$ between the conjugate momenta of the first dissociation step ($OD^+ - D^+$) and the second

dissociation step (O^+–D) is shown in Fig. 10(a). For consistency with panels (b), (c), and (d) that are discussed below, we restricted the polarization vector to be ± 40° within the molecular breakup plane in Fig. 10(a) [31]. The distribution of $\theta_{\mathrm{OD,D}}$ exhibits a peak at ≈ 60°. We can assume that the original bond angle θ(D-O-D) of the neutral D_2O was +104.5°. This value is concomitant with an initial value of +110.4° for $\theta_{\mathrm{OD,D}}$. As such, the measured angle $\theta_{\mathrm{OD,D}}$ in Fig. 10(a) indicates that the OD^+_{II} fragment rotated by ≈ 50° before it dissociated.

During this fast sequential breakup process of the molecular dication, the D^+_I fragment recoils from the OD^+_{II} transient that has a bond-length of ≈ 2.1 bohr for the $A^3\Pi$ state of OH^+ [32] near the FC region. Using the measured final momentum of the D^+_I fragment, depicted in Fig. 3 (≈ 40.6 a.u.), we can deduce how much angular momentum the D^+_I fragment imparted to the OD^+_{II} transient. With this knowledge we can then estimate how long it took the OD^+_{II} fragment to rotate by the observed angle of ≈ 50° (a similar procedure was used for the body-fixed frame electron emission patterns in the PDI of C_2H_2 [33]). To estimate where the kick from the D^+_I fragment is imparted onto the OD^+_{II} rotor, we classically propagated the asymmetric stretch of $OD^+ + D^+$ in time on the PEC. We deduce that it takes ≈ 65 fs for the D^+ fragment to reach the measured 40.6 a.u. of momentum. This is about the same amount of time it took to transform acetylene into vinylidene, as observed in Ref. [33]. Within this time of 65 fs, a rotation of OD^+_{II} by ≈ 50° is reached if the point of contact on OD^+_{II} is located at $R_{average}$ ≈ 61 % of the distance from the center-of-mass of the OD^+_{II} to the oxygen. In our classical picture of a sequential dissociation, which we describe as two successive two-body breakups, this $R_{average}$ represents the average location of the electron hole on OD^+_{II} with which the firstly emitted D^+_I interacts over the time of ≈ 65 fs.

From the two conjugated momenta of the consecutive fragmentation steps, we are also able to derive the dissociation angles with respect to the polarization vector of the first breakup step, D^+_I – OD^+_{II}, in Fig. 10(b), and the second breakup step, O^+ – D_{II}, in Fig. 10(c). For this, we again restricted the polarization vector to be ± 40° within the molecular breakup plane in Fig. 10(b,c). Additionally, we made sure that $\mathbf{p}_{OD^+_{II}}$ and $\mathbf{p}_{OD^+_{II},D^+_I}$ are at positive angles in panel (b) and (c), respectively, in order to visualize the effect of the polarization axis on the orientation of the molecule during the dissociation.

Examining the orientation of the D^+_I – OD^+_{II} breakup axis of the first dissociation step, depicted in Fig. 10(b), a preference for parallel orientation along the polarization vector is observed. A slight tilt of the polarization axis to negative angles is visible. We believe that this slight tilt reflects the change of the point charge location, which is imparted by the D^+_I onto the OD^+_{II} during the OD^+_{II} rotation, stretch, and charge exchange that take place within the ≈ 65 fs. Over the elapsed time between the first (D^+_I + OD^+_{II}) and second (O^+ + D_{II}) dissociation steps, the transient OD^+_{II} has undergone a rotation by ≈ 50° from the assumed original $\theta_{OD,D}$ angle of 110.4°, as visible in Fig. 10(c). The schematic representation in Fig. 10(d) offers a sketch of the successive fast breakup steps with respect to the polarization vector.

We summarize this fast sequential breakup scenario following the direct double ionization of water resulting in high-KER_{OD} as:

SCENARIO (III): SOC and charge exchange during fast sequential breakup

1) $D_2O^{2+}(1^3A_2, 1^3B_2) \xrightarrow{asym.\ OD\ stretch}$
2) $D^+_I + OD^+_{II}(A^3\Pi) \xrightarrow{\text{atomic SOC}}$
3) $D^+_I + OD^+_{II}(X^3\Sigma^-) \xrightarrow{\text{charge exchange}}$
4) $D^+_I + OD^+_{II}(B^3\Sigma^-) \xrightarrow{OD_{II}\ \text{dissociation}}$
5) $D^+_I + O^+(^4S) + D_{II}$

IV. DISCUSSION

We are now able to recap the three discernable fragmentation routes that lead to the high-KER_{OD} feature of the $D^+ + O^+ + D$ reaction channel and put them in context to each other.

Scenario (I): In the above-considered Scenario (I), which involves the symmetric stretch of D_2O^{2+}, only the 1^1A_1 and 1^1B_1 dication singlet states exhibit shallow wells near the FC region. Therefore, these singlet states are expected to contribute to this direct fragmentation scenario. Yet, we can see in Fig. 2 that both the 1^1A_1 and 1^1B_1 dication states likely contribute only to a small degree at ≈ 9.9% and ≈ 16.3%, respectively, to the overall $D^+ + O^+ + D$ yield. Because of the fragment energy resolution, the fitting procedure is not very sensitive to the contributions to the high-energy tail of the electron sum energy, $E_{e_{sum}}$, and therefore these assessments should be taken into account with some reservation. In conclusion, this reaction pathway, which represents the direct fragmentation via the symmetric stretch of D_2O^{2+}, will likely contribute little to the $D^+ + O^+ + D$ reaction channel with high-KER_{OD} after direct PDI of D_2O with 61 eV photons. This is to be expected, as the direct fragmentation of D_2O^{2+} into $D^+ + D^+ + O$ is a fast process, which offers little time for effective SOC under only select kinematics to change the course of the reaction. Lower KER and larger emission angles $\phi_{D^+,D}$ between the D^+ ion and D fragment along with smaller emission angles $\phi_{O^+,D}$ between the O^+ ion and the D fragment increase the chances for effective electron transfer in the direct fragmentation of the 1^1B_1 dication state. Such favorable kinematic conditions are not present in the high-KER_{OD} case discussed here (see Fig. 4), but play a small role in the low-KER_{OD} case [10]. This direct fragmentation scenario of the low-KER_{OD} contribution, fed by mostly

the 1^1B_1 dication state, is discussed in Ref. [10] as a minor contributor ($\leq$ 16%) to the $D^+ + O^+ + D$ production.

Scenario (II): This scenario can be seen as a variant of Scenario (I). Instead of a SOC-enabled direct breakup upon symmetric stretch of the water dication, Scenario (II) involves a small asymmetric stretch ($R_{(2)} = R_{(1)}$ - 1 bohr). We expected the 1^1A_2 and (to a lesser degree) the 2^1A_1 dication states to play a role in Scenario (II). However, despite the favorable energetics for both states, an analysis of the spin-orbit matrix elements enabled us to eliminate the 2^1A_1 dication state from consideration, leaving the 1^1A_2 state as the sole player in this breakup scenario. The multi-Gaussian fit (see Fig. 2) estimates the high-KER contribution of the 1^1A_2 dication state to the $D^+ + O^+ + D$ production to be at most 23.9%. This breakup mechanism requires electron transfer, which proceeds on a short seam of intersection between the 1^1A_2 and 2^3A_2 states via SOC. As we see in Fig. 5, the seam of intersection between the 1^1A_2 state and the 2^3A_2 state extends over several bohr and yields both time and phase-space for a more efficient electron transfer in this fragmentation pathway. Moreover, we found that the region of coordinate space where the seam of intersection resides is energetically downhill from the FC region where PDI is initiated (see Fig. 6).

Scenario (III): The third fragmentation route Scenario (III), i.e., the fast-sequential breakup involving atomic SOC and charge exchange within the transient OD^+_{II} ion, which supports transitions at bigger asymmetric stretches than Scenario (II) ($\gtrsim$7 bohr instead of $\approx$ 5 bohr), is dominated by the 1^3A_2 and 1^3B_2 dication states. It is also conceivable that this fragmentation is exclusively responsible for the entire high-KER_{OD} feature of the $D^+ + O^+ + D$ reaction channel upon direct PDI. The 1^3A_2 and 1^3B_2 dication states, which can only play a role in this fast-sequential breakup scenario, already contribute with 49.9% and 23.9%, respectively, according to the measured electrons sum energy shown in Fig. 2. However, the 23.9% is a shared contribution between 1^3B_2 dication state of scenario (III) and the 1^1A_2 dication state of scenario (II), since, in our experiment, these two states cannot be separated using the electrons sum energy, as discussed in Sec. III A.

Accordingly, it is this Scenario (III) of a fast-sequential breakup that contributes the most to the high-KER_{OD} feature in the $D^+ + O^+ + D$ reaction channel. It is important to stress that the 1^3A_2 and 1^3B_2 dication triplet states did not play an important role in the slow-sequential dissociation producing the $D^+ + D^+ + O$ breakup channel, as discussed in our previous work [14]. However, for the fast-sequential breakup discussed here that is generating $D^+_I + O^+ + D_{II}$, the 1^3A_2 and 1^3B_2 states contribute substantially [on a relative scale] to the OD^+_{II} breakup into $D_{II} + O^+(^4S)$, since those two triplet dication states can fragment directly into $OD^+_{II}(A^3\Pi)$ transient fragment ions at an intermediate asymmetric stretch ($\gtrsim$7 bohr) without the need for SOC. Moreover, as a crucial coupling within the intermediate OD^+_{II} fragment can populate the X state, wherein the firstly emitted D^+_I ion acts as a spectator, larger and more asymmetric stretch scenarios are accessed, allowing charge-exchange from the X state of OD^+_{II} to the $B^3\Sigma^-$ state over a long range of O-D_{II} separations in the intermediate regime to take place. Both of these favorable conditions are reflected in the high relative contribution of the 1^3A_2 and 1^3B_2 dication states to the $D^+_I + O^+ + D_{II}$ production via fast sequential fragmentation [see Fig. 2]. The same fast sequential dissociation process via the 1^3A_2 dication state also contributed at 20.4% in the low-KER_{OD} events that are presented in Ref. [10].

The time between the first and second dissociation step in this fast sequential breakup Scenario (III) was deduced to be around 65 fs. For this fragmentation route to happen efficiently, the OD bond, which breaks first and expels the D^+_I ion, is preferentially aligned along the direction of the linear polarization vector. Assuming that the deuterated water molecular dication exhibited a bond angle of around 104.5°, which corresponds to an initial $\theta_{OD,D}$ angle of 110.4°, the OD^+_{II} fragment rotated by $\approx$ 50°, resulting in a closing of the $\theta_{OD,D}$ angle from 110.4° to $\approx$ 60°. A preference for parallel orientation of the D^+_I – OD^+_{II} breakup axis along the polarization vector of light is also observed with an apparent small tilt, which we believe is due to the change of the point charge location in OD^+_{II} during the dissociation process.

We must stress that the observed dynamics of this dissociation process, which happens on an ultrafast timescale, limits the accuracy of the native frame core assumption of two distinct decoupled dissociation steps. Furthermore, Scenario (III) involves a charge transfer that results in a switch of Coulomb field interactions from D^+_I – D^+_{II} to D^+_I – O^+ during the dissociation process. This charge transfer impacts the trajectory of the fragments, consequently affecting their measured final momenta. Therefore, the separation into a sequence of two two-body interactions, as employed in the native frame analysis method, is only a simplification for Scenario (III). Accurately describing the three-body dynamics of this Scenario (III) requires calculations on the relevant multi-dimensional PES, which currently presents a significant challenge for electronic structure methods applied to this fundamentally important system [34].

In Table I, we summarize this discussion with a listing of all the valence states of D_2O^{2+} populated by a 61 eV photon in a direct PDI, their vertical energies in ascending order, and the role they play in the $O^+(^4S)$ production with high- and low-KER_{OD}.

V. SUMMARY

Absorbing a single 61 eV (± 0.2 eV) linearly-polarized photon in D_2O populates the six electronically excited

TABLE I. Vertical energies (VE) in [eV] of the lowest dication states measured with respect to the X^3B_1 state at the equilibrium geometry of neutral water for the high-KER_{OD} (this work) and low-KER_{OD} ([10]) contribution of the water dication breakup. Note that the relative yields of the high-KER_{OD} ($KER_{OD} > 0.25$ eV) and low-KER_{OD} ($KER_{OD} \leq 0.25$ eV) contributions for the direct PDI with 61 eV of D_2O, resulting in the $D^+ + O^+ + D$ channel, are 53.2% ± 5% and 46.8% ± 5%, respectively. The role of each state in the O^+ production is indicated. "Scen. (I) to (III)" refer to the breakup processes discussed in this work. "Scen. (1)" refers to the direct fragmentation, "Scen. (2)" to the slow sequential fragmentation, and "Scen. (3)" to the fast sequential fragmentation as explained in Ref. [10].

Contribution	State	VE	Role	Reference	Yield
high-KER_{OD}	1^1A_1	1.2	sym. stretch 3-body frag. through shallow well	Scen. (I)	9.9% ± 0.5%
	1^1B_1	2.6	sym. stretch 3-body frag. through shallow well	Scen. (I)	16.3% ± 0.7%
	1^3A_2	4.3	fast-seq. frag.	Scen. (III)	49.9% ± 0.6%
	1^1A_2	6.5	small asym. stret. 3-body frag. via SOC on seam to 2^3A_2	Scen. (II)	23.9% ± 0.5%[a]
	1^3B_2	6.5	fast-seq. frag. as with 1^3A_2	Scen. (III)	
low-KER_{OD}	1^1B_1	2.6	slow 2-body seq. frag. to $OH^+(a^1\Delta)$	Scen. (1) & (2) in Ref. [10]	55.4% ± 0.9%
	1^3A_2	4.3	fast-seq. frag.	Scen. (3) in Ref. [10]	24.2% ± 1.2%
	2^1A_1	5.8	slow 2-body seq. frag. to $OH^+(b^1\Sigma^+)$	Scen. (2) in Ref. [10]	20.4% ± 1%

[a] The contributions from the 1^1A_2 and 1^3B_2 dication states cannot be separated in our measurement.

dication states 1^1A_1, 1^1B_1, 1^3A_2, 1^3B_2, 2^1A_1, and 1^1A_2 in the direct PDI. Some of these water dications dissociate via the rare $D^+ + O^+(^4S) + D$ fragmentation channel. In this report, we focused on the events with high $KER_{OD} \geq 0.25$ eV via symmetric stretch and small as well as large asymmetric stretch of D_2O^{2+} (with SOCs at ≈ 5 bohr, ≈ 5.5 bohr, and ≥ 7 bohr, respectively). We conclude that direct three-body fragmentation via SOC following symmetric stretch [Scenario (I)] and small asymmetric stretch [Scenario (II)] plays only a minor role and that the fast sequential dissociation process [Scenario (III)] dominates the reaction dynamics.

This state-selective, highly differential investigation on the three-body fragmentation of water, resulting in the high-KER_{OD} contribution of $D^+ + O^+ + D$ upon direct PDI, reveals the rivalry and dynamics of (deuterated) water dication states feeding different two- and three-body intermediate reaction channels and elucidates the competition between three multi-step dissociation scenarios with symmetric and asymmetric DOD stretches that involve SOC. Only the combination of highly differential experimental and detailed theoretical investigations enabled us to trace and time these scarce ultrafast dissociation pathways in this fundamental triatomic system and elucidate the role of SOC on the PESs. An analogous electron transfer at similar intermediate distances (≈ 18 bohr), without the need for SOC and, hence, greater efficiency, has been observed recently in the PDI of NH_3 [35].

Overall, we find six active dication states after direct PDI that produce the rare $D^+ + O^+ + D$ fragmentation channel with high- and low-KER_{OD} [10] via six different dissociation scenarios (see Table. I). As such, our investigation exemplifies the rich and diverse competing ultrafast dynamics in a small prototypical polyatomic molecule, which is triggered by a narrow-bandwidth light pulse and results in the same outcome but via different short- and long-lived intermediates. Electron transfer via SOC markedly influences the likelihood of each individual dissociation pathway along the bend and stretch modes on the PESs and their seams. We believe our findings will be useful for designing future pump-probe experiments on (time-resolved) excited-state dissociation dynamics of water and other small polyatomic molecules using tabletop lasers or fourth-generation light sources to further confirm such rapid dissociation steps that depend on SOC and elucidate their dynamics in real-time investigations.

ACKNOWLEDGMENTS

We thank T. Weinacht for sparking our interest in this scarce water fragmentation channel. Work at LBNL was supported by the U.S. Department of Energy (DOE), Office of Science, Basic Energy Sciences (BES) under Award No. DE-AC02-05CH11231. This research used resources of the Advanced Light Source (ALS) and the National Energy Research Scientific Computing Center (NERSC), both being DOE Office of Science User Facilities under contract No. DE-AC02-05CH11231. In particular we acknowledge NERSC award BES-ERCAP-0020143 (theory) and BES-ERCAP-0019776 (experiment). We thank the staff of the ALS, in particular beamline 10.0.1 for their outstanding support. The JRML personnel was supported by the U.S. Department of Energy (DOE), Office of Science, Basic Energy Sciences (BES) under Award No. DE-FG02-86ER13491. UNR personnel acknowledges support from the National Sciences Foundation under Award No. NSF-1807017 and NSF-2208017. We are indebted to the RoentDek Company for long-term support with detector software and hardware.

CONFLICTS OF INTEREST

The authors have no conflicts to disclose.

AUTHOR CONTRIBUTIONS

W. I. and Th. W designed the experiment. W. I., Th. W., K.A. L., B. G., J.B. W., B. J., D. C., V. D., T. S., and D.S. S. conducted the beam time and acquired the experimental data at the Advanced Light Source. W. I. analyzed the data. T.N. R., A.E. O., and Z.L. S. performed the calculations. W. I., T.N. R, and Th. W. wrote the manuscript with significant review and editing by D.S. S., R.R. L., C.W. McC., and I. B-I., which all coauthors approved. W. I., T.N. R., and Th. W. created the figures.

DATA AVAILABILITY

The data-sets generated during the current study are available from the corresponding authors upon reasonable request.

[1] M. Born and R. Oppenheimer, Ann. Phys. **84**, 0457 (1927).
[2] D. R. Yarkony, Rev. Mod. Phys. **68**, 985 (1996).
[3] W. Domcke, D. R. Yarkony, and H. Köppel, Adv. Series in Phys. Chem, Conical Intersections: Electronic Structure, Dynamics and Spectroscopy **15**, 856 (2004).
[4] B. F. E. Curchod and T. J. Martinez, Chem. Rev. **118**, 3305 (2018).
[5] L. Zhang, Y. Shu, S. Sun, and D. G. Truhlar, J. Chem. Phys. **154**, 094310 (2021).
[6] C. M. Marian, Wiley Interdiscip. Rev.: Comput. Mol. Sci. **2**, 187 (2012).
[7] C. M. Marian, Annu. Rev. Phys. Chem. **72**, 617 (2021).
[8] S. Mukherjee, D. A. Fedorov, and S. A. Varganov, Annu. Rev. Phys. Chem. **72**, 515 (2021).
[9] F. Fritsch, T. Weike, , and W. Eisfeld, J. Chem. Phys. **156**, 054115 (2022).
[10] W. Iskandar, T. N. Rescigno, A. E. Orel, T. Severt, K. A. Larsen, Z. L. Streeter, B. Jochim, B. Griffin, D. Call, V. Davis, C. W. McCurdy, R. R. Lucchese, J. B. Williams, I. Ben-Itzhak, D. S. Slaughter, and T. Weber, J. Chem. Phys. **159**, 094301 (2023).
[11] H. Sann, T. Jahnke, T. Havermeier, K. Kreidi, C. Stuck, M. Meckel, M. S. Schöffler, N. Neumann, R. Wallauer, S. Voss, A. Czasch, O. Jagutzki, T. Weber, H. Schmidt-Böcking, S. Miyabe, D. J. Haxton, A. E. Orel, T. N. Rescigno, and R. Dörner, Phys. Rev. Lett. **106**, 133001 (2011).
[12] Z. L. Streeter, F. L. Yip, R. R. Lucchese, B. Gervais, T. N. Rescigno, and C. W. McCurdy, Phys. Rev. A **98**, 053429 (2018).
[13] D. Reedy, J. B. William, B. Gaire, A. Gatton, M. Weller, A. Menssen, T. Bauer, K. Henrichs, P. Burzunski, B. Berry, Z. L. Streeter, J. Sartor, I. Ben-Itzhak, T. Jahnke, R. Dörner, T. Weber, and A. L. Landers, Phys. Rev. A **98**, 053430 (2018).
[14] T. Severt, Z. L. Streeter, W. Iskandar, K. A. Larsen, A. Gatton, D. Trabert, B. Jochim, B. Griffin, E. G. Champenois, M. M. Brister, D. Reedy, D. Call, R. Strom, A. L. Landers, R. Dörner, J. B. Williams, D. S. Slaughter, R. R. Lucchese, T. Weber, C. W. McCurdy, and I. Ben-Itzhak, Nat. Commun. **13**, 1763 (2022).
[15] G. Olivera, C. Caraby, P. Jardin, A. Cassimi, L. Adoui, and B. Gervais, Phys. Med. Biol. **43**, 2347 (1998).
[16] K. H. Tan, C. E. Brion, P. E. V. der Leeuw, and M. J. van der Wiel, Chem. Phys. **29**, 299 (1978).
[17] P. J. Richardson, J. H. D. Eland, P. G. Fournier, and D. L. Cooper, J. Chem. Phys. **84**, 3189 (1986).
[18] D. Winkoun, D. Dujardin, L. Hellner, and M. J. Besnard, J. Phys. B **21**, 1385 (1988).
[19] M. N. Piancastelli, A. Hempelmann, F. Heiser, O. Gessner, A. Rüdel, and U. Becker, Phys. Rev. A **59**, 300 (1999).
[20] J. D. Eland, Chem. Phys. **323**, 391 (2006).
[21] J. Laksman, E. P. Mansson, A. Sankari, D. Ceolin, M. Gisselbrecht, and S. L. Sorenson, Phys. Chem. Chem. Phys. **15**, 19322 (2013).
[22] W. Iskandar, T. N. Rescigno, A. E. Orel, K. A. Larsen, B. Griffin, D. Call, V. Davis, B. Jochim, T. Severt, J. B. Williams, I. Ben-Itzhak, D. S. Slaughter, and T. Weber, Phys. Chem. Chem. Phys. **25**, 21562 (2023).
[23] A. Zulfiqar, Y.-D. Chuang, D. Kilcoyne, A. Aguilar, S. K. Mo, and Z. Hussain, Proc. SPIE **8502**, 85020P (2012).
[24] R. Dörner, V. Mergel, O. Jagutzki, L. Spielberger, J. Ullrich, R. Moshammer, and H. Schmidt-Böcking, Phys. Rep. **330**, 95 (2000).
[25] J. Ullrich, R. Moshammer, A. Dorn, R. Dörner, L. P. H. Schmidt, and H. Schmidt-Böcking, Rep. Prog. Phys. **66**, 1463 (2003).
[26] T. Jahnke, T. Weber, T. Osipov, A. L. Landers, O. Jagutzki, L. P. H. Schmidt, C. L. Cocke, M. H. Prior, H. Schmidt-Böcking, and R. Dörner, J. Electron Spectrosc. Relat. Phenom. **141**, 229 (2004).
[27] R. Dörner, T. Weber, M. Achler, V. Mergel, L. Spielberger, O. Jaguzki, F. Afaneh, M. H. Prior, C. L. Cocke, and H. Schmidt-Böcking, *Imaging in Chemical Dynamics (ACS Symposium Series)* (eds. A.G. Suits and R.E. Continetti, Oxford, 2000) p. 339.
[28] O. Jagutzki, A. Cerezo, A. Czasch, R. Dörner, M. Hattass, M. Huang, V. Mergel, U. Spillman, K. Ullmann-Pfleger, T. Weber, H. Schmidt-Böcking, and G. D. W. Smith, IEEE Trans. Nucl. Sci. **49**, 2477 (2002).
[29] B. Gervais, E. Giglio, L. Adoui, A. Cassimi, D. Duflot, and M. E. Galassi, J. Chem. Phys. **131**, 024302 (2009).
[30] J. Rajput, T. Severt, B. Berry, B. Jochim, P. Feizollah, B. Kaderiya, M. Zohrabi, U. Ablikim, F. Ziaee, K. Raju, D. Rolles, A. Rudenko, K. D. Carnes, B. D. Esry, and I. Ben-Itzhak, Phys. Rev. Lett. **120**, 103001 (2018).
[31] Removing this condition results in no notable change in the angular distribution depicted in Fig. 10(a).
[32] R. P. Saxon and B. Liu, J. Chem. Phys. **85**, 2099 (1986).
[33] T. Osipov, C. L. Cocke, M. H. Prior, A. Landers, T. Weber, O. Jagutzki, L. Schmidt, H. Schmidt-Böcking, and R. Dörner, Phys. Rev. Lett. **90**, 233002 (2003).
[34] We point out that for small polyatomic molecules like water, multiple-spawning surface dynamics and non-

adiabatic ab initio molecular dynamics (AIMD) methods, where electronic energies, gradients, and non-adiabatic coupling matrix elements (NACMEs) are computed on-the-fly [see, e.g., B. F. E Curchod and T. J. Martinez, Chem. Rev. **118**, 3305 (2018), and K. Gope et al., J. Phys. Chem. Lett. **11**, 8108 (2020)] can be applied as an alternative theory approach to further investigate this dissociation channel.

[35] K. Larsen, T. N. Rescigno, T. Severt, Z. L. Streeter, W. Iskandar, S. Heck, A. Gatton, E. G. Champenois, R. Strom, B, Jochim, D. Reedy, D. Call, R. Moshammer, R. Dörner, A. L. Landers, J. B. Williams, C. W. McCurdy, R. R. Lucchese, I. Ben-Itzhak, D. S. Slaughter, and T. Weber, Phys. Rev. Research **2**, 043056 (2020).